Journal of Heat and Mass Transfer Research

Journal homepage: https://jhmtr.semnan.ac.ir

Semnan University

ISSN: 2383-3068

Research Article

Comparison of Different Turbulent Models in Flow on a Rotating Airfoil Considering Centrifugal Acceleration Force, Coriolis Force and Thermal Dissipation

Iraj Fazeli Farsani, Bahman Asadi *

Mechanical Engineering Group, Golpayegan College of Engineering, Isfahan University of Technology, Golpayegan, 8771767498, Iran

ARTICLE INFO

Article history:

Received: 2023-05-15

Revised: 2024-07-08

Accepted: 2024-07-08

Keywords:

Rotating airfoil;

Coriolis;

RANS;

LES.

ABSTRACT

The moving blades in a circular path have many industrial applications, in more modern turbo machines, such as jet engine compressors, the flow conditions are completely incompressible. On the other hand, the 2D study of the flow around these blades, which shows many characteristics of the flow and simplifies the matter, is usually unavoidable. In this regard, the simulation methods LES and RANS, in order to simulate the flow around the NACA0012 airfoil, different modes of fixed and rotating airfoil with different angles of attack and 3D impeller mode have been implemented. The lift coefficient, drag coefficient, torque, and mass flow of S-A, RNG, SST, RSM, and LES models are compared. The net mass rate will be different in the above methods. In RANS methods, the value of the net mass rate is negative; that is, loss of mass rate occurs, but in the LES method, the value of the net mass rate is positive. The highest net mass rate is related to the LES method, and in RANS models, the reverse flow is observed. According to the results, the effects of body forces in energy equation or thermal dissipation under circular motion are important in comparison with experimental data. A comparison of fixed and rotating airfoil lift coefficient diagrams with the LES model shows that the lift coefficient in a fixed airfoil is two times relative to a rotating airfoil. Also, the torque on the impeller, compared with different turbulent models, varies from 88381 to 172116.

1. Introduction

Proper airfoil design is of utmost importance in order to satisfy technical and economic aircraft design requirements. Efficient airfoils can enable aircraft to carry heavier loads, fly at faster speeds, and decrease fuel consumption. One widely used metric for evaluating an airfoil's performance is the lift/drag ratio, which is calculated by dividing the airfoil's lift coefficient by the drag coefficient. Improving the aerodynamic performance of airfoils is a vital area of research for the design of next-generation airplanes.

In recent years, advances in computing power have enabled the rapid proliferation of computational fluid dynamics (CFD) techniques. CFD simulation is becoming one of the most important parts of aerodynamic and fluid mechanics industries. Almost all aerodynamic cases that exist in our world have a connection with fluid dynamics. For the analysis of moving cases (or flow around objects) in CFD toolboxes, there exist some hypothetical models for turbulent simulation.

In this paper, turbulent viscous flow around a moving airfoil on a circular path is simulated. A

* **Corresponding author.**
E-mail address: b.asadi@iut.ac.i

Cite this article as:
Fazeli Farsani, I. and Asadi, B., 2024. Comparison of Different Turbulent Models in Flow on a Rotating Airfoil Considering Centrifugal Acceleration Force, Coriolis Force and Thermal Dissipation. *Journal of Heat and Mass Transfer Research*, 11(2), pp. 285-296.
https://doi.org/10.22075/JHMTR.2024.30533.1443

cylindrical grid is used. Non-rotating airfoil was used for accuracy and comparison with experimental results. Previous work in this field includes the following cases:

Steenwijk et al. [1] Numerical study of turbulent flows over a NACA0012 airfoil: insights into its performance and the addition of a slotted flap. The airflow around a 2D NACA 0012 airfoil at various angles of attack is simulated using the RANS SST turbulent flow model and compared to experimental data. Results match the behavior expected from wing theory well, showing how CFD can be effectively applied in the development and optimization of wings, flaps, and wingtips.

Silva et al. [2] analyzed the effects of adverse pressure gradient in the boundary layer of NACA0012 airfoil at high angles of attack. The LES is performed for a NACA0012 airfoil at 9 deg. angle of attack, Reynolds number Re = 400, 000 and Mach number M = 0.2. Results are first presented in terms of aerodynamic coefficients and integral quantities. The APGs are shown to impact the turbulence statistics, especially the Reynolds stress distributions and, subsequently, the production, dissipation, and pressure diffusion terms of the TKE budgets.

Silva et al. [3] investigated the shear layers embedded in the turbulent boundary layers of a NACA0012 airfoil at high angles of attack. an investigation of turbulent boundary layers (TBLs) is presented for a NACA0012 airfoil at angles of attack 9 and 12 deg. Wall-resolved large eddy simulations (LES) are conducted for a freestream Mach number M = 0.2 and chord-based Reynolds number Re = 4x105, where the boundary layers are tripped near the airfoil leading edge on the suction side. The analysis of the turbulence production shows that other components of the production tensor become important in the outer layer besides the shear term. For moderate and strong APGs, the mean velocity profiles depict three inflection points, the third being unstable under inviscid stability criteria.

Sharma et al. [4] numerical simulation and validation of NACA0012 airfoil to predict its performance in stall conditions. In this article, the effect of changing the angle of attack on a single-bladed airfoil with a medium Reynolds number is investigated with the SST-SAS turbulence model. The coefficient of lift and drag performance metrics have also been investigated for critical angles of attack, and the findings demonstrate good agreement with the experimental data of the literature.

Rahimi et al [5] investigated numerically the convective heat transfer from the horizontal plane due to the oscillation of the vertical blade. Numerical analysis was performed using commercial software ANSYS Fluent 6.3, and the periodic oscillation of the blade was modeled using the moving mesh method. The effect of various parameters, including the amplitude and frequency of the blade oscillation as well as the geometrical parameters, was investigated on the convective heat transfer from the target plate. The results indicated that a wider area of the plate was affected by increasing the oscillation amplitude of the blade. Convective heat transfer was also enhanced over the entire target plate as the rotational Reynolds number was increased.

Mitchell et al. [6] studied the aerodynamic properties of NACA0012 airfoil and predicted the performance of wind turbines by calculating aerodynamic forces with RANS and LES models at different angles of attack. It is not able to reproduce vortex propagation and vortex formation, but the LES model is well consistent with experimental results.

Balakumar [7] studied the flow on high-Reynolds NACA0012 airfoil using the LES wall model and compared the results with the existing DNS26 and experimental reference datasets, which showed that the pressure distribution and friction coefficient were good agreement with the DNS Rizzetta and Visbal Data. However, the turbulence intensity and shear stresses of the WMLES model are predicted to be too much compared to the DNS near the end edge.

Zhao et al. [8] simulated the cavitation around the NACA0012 airfoil using SST, K-omega, and LES Smagorinsky models. Then, the simulation results, such as cavitation shape, drop and lift frequency, and lift and drag coefficients, compared the three models of analysis turbulence with each other and the experimental results. The results showed that the Smagorinsky model of the LES method is able to provide specific information about the cavitation flow that the RANS method has failed.

Oukassou et al. [9] simulated 2-D flow around the NACA0012 and NACA2412 airfoils at Reynolds numbers and different attack angles. They compared the lift, drag, and pressure coefficients using the three models Spalart-Allmaras, k-epsilon (RNG), and k-omega (SST) with the experimental results in the wind tunnel of the National Aviation Consulting Association. Overall, they found good agreement.

Filomena et al. [10] simultaneously investigated a fixed-winged multi-finned locust in which only the force due to Coriolis acceleration was added to the term of the Navier-Stokes momentum equation for faster convergence. The results were in good agreement with the experimental data in the impeller performance range, and the computational results clearly showed the effect of rotation speed and the increase of total pressure on the spinner and the wing.

Eleni et al. [11] evaluated the Spalart-Almaras, K-Epsilon, and ST-K omega turbulence models to simulate the flow on a 3 million Reynolds Reynolds airfoil with ultrasonic flow and 2D mode. Their aim was to investigate the airfoil behavior in those conditions and validate the turbulence methods and models by predicting and comparing them with laboratory results. Their computational range includes 80,000 grids near the wall in order to properly capture the boundary layer. Eleni and colleagues found that the turbulence models used in commercial computational fluid dynamics codes were not yet able to display accurate results at high attack angles.

Sipilä et al. [12] discussed the effects of oscillating currents around propellers and provided researchers with valuable results in the field of current-induced vibrations. In fact, vibrations in the blades are one of the causes of current turbulence. This has its advantages and disadvantages.

Qiu et al. [13] investigated the effects on the locust tips by the RANS method and presented the desired results in the field of turbulence in the blade tips. The tip of the blade is one of the causes of rotational current and turbulence in the current. In this research, an attempt has been made to show how the current separates.

Abbott et al. [14] conducted a laboratory study of the design of NACA0012 airfoils and provided a complete summary of their observations, including wing shear data, wing characteristics, and diagrams of lift, drag, and so on.

Asadi et al. [15] studied the viscous compressible flow around the moving airfoil with different RANS methods and extracted diagrams of pressure coefficient and shell friction for different angles of attack and velocity contour along the impeller and how vortices are formed.

As reviewed in the review articles, the study of the flow around the airfoil has been studied in many articles since about 1985 using different models, but in this article using the airfoil with circular motion and adding centrifugal forces and Coriolis forces, including the source term of momentum equation in Navier-Stokes, the finite volume method, the pressure-based solution, the vector decomposition method have been used. It is worth noting that due to the mobility of the borders, moving grids can be used, but according to the rules of galley transfer, the issue can be investigated from the perspective of a moving (non-inertial) observer by adding terms due to centrifugal forces and Coriolis forces. And reduce the complexity of the moving grid. The purpose of solving turbulent viscous flow with different RANS and LES turbulence models around the desired airfoil is to obtain coefficients for life, Drag, velocity, pressure, and pressure and velocity change diagrams along the impeller as well as contour of velocity and pressure and how to distribute the fluid rotates around the impeller.

2. Numerical Model

The general Navier-Stokes equations for rotational flows are expressed in Eq.1 to 3 [16]:

$$\frac{\partial \rho}{\sigma t} + \nabla.\rho\bar{v}_r = 0 \quad (1)$$

$$\frac{\partial}{\sigma t}\rho\bar{v} + \nabla.(\rho\bar{v}_r\bar{v}) + \rho[\bar{\omega} \times (\bar{v} - \bar{v}_t)] = -\nabla\rho + \nabla.\bar{\tau} + \bar{F} \quad (2)$$

$$\frac{\partial}{\sigma t}\rho E + \nabla.(\rho\bar{v}_r H + \rho\bar{u}_r) = \nabla.(K\nabla T + \bar{\tau}.v) + S_h \quad (3)$$

The general form of the Navier-Stokes equations is summarized in Eq.4 in the vector form of the above equations [15]:

$$\frac{\partial \bar{x}}{\partial t} + \nabla\bar{F}_l + \nabla\bar{F}_V = \bar{Q}_x \quad (4)$$

Where the X vector is defined as Eq.5 [16]:

$$\bar{X} = \begin{bmatrix} \rho \\ \overline{\rho v} \\ \rho E \end{bmatrix} \quad (5)$$

In the above equations, Fi and Fv are flux-related vectors that are defined as Eq.6 and 7 [16].

$$F_{li} = \begin{bmatrix} \rho v_i \\ \rho v_1 v_i + \rho\delta_{1i} \\ \rho v_2 v_i + \rho\delta_{2i} \\ \rho v_3 v_i + \rho\delta_{3i} \\ (\rho E + P)v_i \end{bmatrix} \quad (6)$$

$$-F_{vi} = \begin{bmatrix} 0 \\ \tau_{i1} \\ \tau_{i2} \\ \tau_{i3} \\ q_i + v_j\tau_{ij} \end{bmatrix} \quad (7)$$

Q is a vector that is added to the source [16].

$$\overline{\mathrm{Q}}_{\mathrm{x}} = \begin{bmatrix} 0 \\ \rho\bar{f}_e \\ W_f \end{bmatrix} \quad (8)$$

That Wf is the work of the body forces appearing in the momentum equation. Which is expressed Eq.9 [16]:

$$W_f = \rho\bar{f}_e v \quad (9)$$

$$\overline{Q_x} = \begin{bmatrix} 0 \\ -\rho(\overline{w} \times \bar{v}) \\ 0 \end{bmatrix} \quad (10)$$

Q can also be defined as Eq.10 [16].

2.1. RANS Model Equations

Time averaged Navier-Stokes equations is averaged by Reynolds Method in continuity, momentum and the energy equation, which is written in following form for Newtonian fluid in tensor form [17]:

$$\frac{\partial \bar{u}_j}{\partial x_j} = 0 \tag{11}$$

$$\frac{\partial}{\partial x_j}\left(\rho \bar{u}_i \bar{u}_j\right) = -\frac{\partial}{\partial x_i}\left(\bar{p} + \frac{2}{3}\rho k\right) + \frac{\partial}{\partial x_j}\left\{\mu_{eff}\left(\frac{\partial \bar{u}_i}{\partial x_j} + \frac{\partial \bar{u}_j}{\partial x_i}\right)\right\} \tag{12}$$

$$\frac{\partial}{\partial x_j}\left(\rho \bar{u}_j \bar{T}\right) = \frac{\partial}{\partial x_j}\left(\Gamma_{eff}\frac{\partial \bar{T}}{\partial x_j}\right) \tag{13}$$

2.2. LES Model Equations

Fluid motion is described by the laws of mass conservation and momentum conservation. The equations of mass and momentum are obtained by the following equations [18].

$$\frac{\partial U_i}{\partial x_i} = 0 \tag{14}$$

$$\frac{\partial U_i}{\partial t} + \frac{\partial U_i U_j}{\partial x_j} = -\frac{1}{\rho}\frac{\partial p}{\partial x_i} + \frac{\partial}{\partial x_j}\left(\upsilon \frac{\partial U_i}{\partial x_j}\right) \tag{15}$$

$$\frac{\partial U_i}{\partial t} + \frac{\partial U_i U_j}{\partial x_j} = -\frac{1}{\rho}\frac{\partial \rho}{\partial x_i} + \frac{\partial}{\partial x_j}\left(\nu \frac{\partial U_i}{\partial x_j}\right) \tag{16}$$

In the simulation of large scale, the filter operator is used to separate each variable ϕ that (ϕ=U.V.W.P) is denoted by scales and small scales (subnets) are denoted by:

$$\phi = \bar{\phi} + \varphi \tag{17}$$

There is an important difference between the RANS and LES models in the type of these operators. In RANS, a time averaging operator is applied to the governing equations, but the operator used in LES is a time-independent local spatial filter [18].

3. Problem Geometry

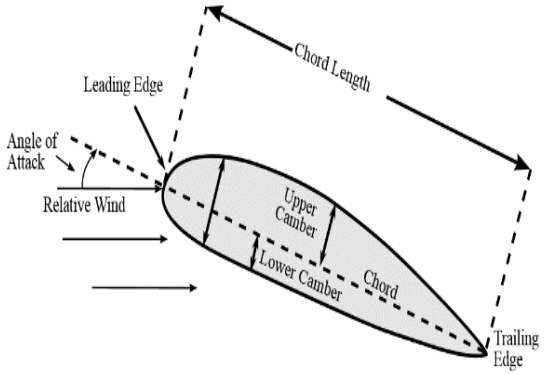

Fig. 1. Schematic of airfoil and problem geometry [19]

3.1. Fixed Airfoil

The 2D turbulent viscous flow around the NACA0012 fixed airfoil in the open air (ideal gas) and the airfoil body is defined as a wall (Wall), and the Pressure-Far-Field geometry environment is considered as shown in Fig. 2.

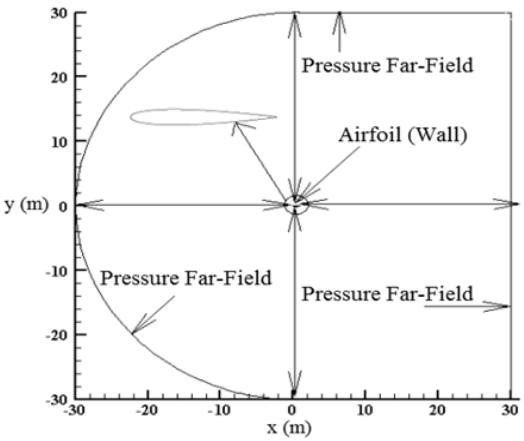

Fig. 2. Geometry and boundary conditions of the problem for fixed airfoil.

3.2. Rotating Airfoil

The 2D turbulent viscous flow around the NACA0012 cross-section airfoil in the open air (ideal gas) rotates around the point (0, 0) at an angle of 24 rpm, and the boundary conditions are as shown in Fig.3.

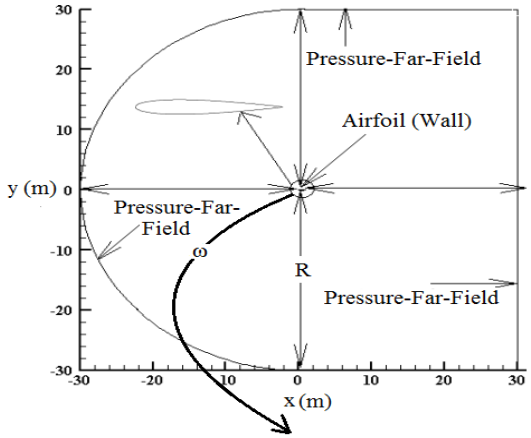

Fig. 3. Problem geometry and boundary conditions for rotating airfoil

3.3. Impeller

The 3D turbulent flow around the impeller with a speed of 21.2 rpm and an inlet velocity of 12 m/s and an outlet with a pressure of 1 atm, and other conditions are in accordance with Fig. 4 This mode is actually a simulator of rotating propeller motion in turbines, airplanes, helicopters.

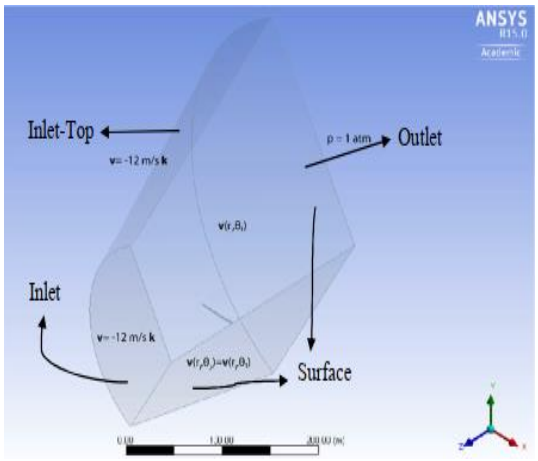

Fig. 4. 3D Impeller Specifications

4. Mesh Independency

Because the geometry of the NACA0012 airfoil is symmetric, this simulation uses an organized grid to create a computational range. The sizes of the grid in the areas close to the airfoil wall and next to it play a key role in creating its flow and dynamics mechanisms. Therefore, it has been tried to make the produced grids completely square and perpendicular to the airfoil wall and tangential to it. Also, due to the limited costs and time and memory of the computer, it is forced to calculate the optimal mode of gridding, and the thickness of the first mesh and the mesh expansion coefficient of 1.2 has been selected. In order to obtain the optimal gridding that can provide accurate predictions about the problem, eight different grids are considered, which can be seen in Table 1:

Table 1. Mesh values

Cases	Number
1	15600
2	21960
3	36000
4	52520
5	72000
6	95880
7	121600
8	152040

According to the result of Fig. 5, the number of points equal to case 7 in Table 1 is considered as the optimal grid size in the continuation of the paper because the changes in turbulent kinetic energy (k) and turbulent dissipation rate (ε) in the last few grids have remained almost constant. The grid is chosen in such a way that the grid near the airfoil wall is considered smaller, and the closer it is to the problem boundaries, the larger the grid is, as shown in Figures 6 and 7.

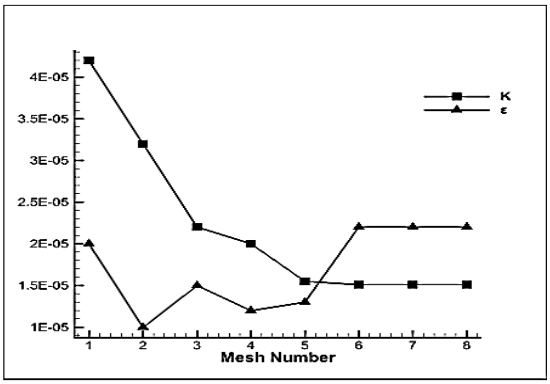

Fig. 5. Changes k and ε for 8 different grid

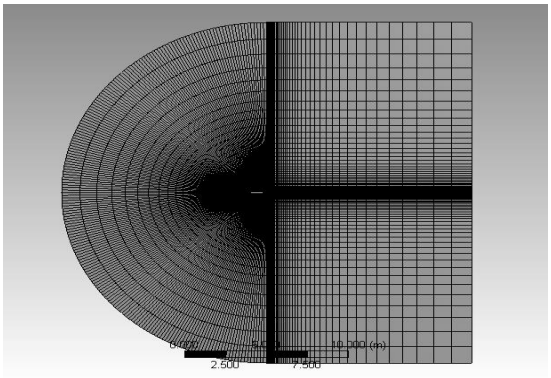

Fig. 6. View of the problem mesh

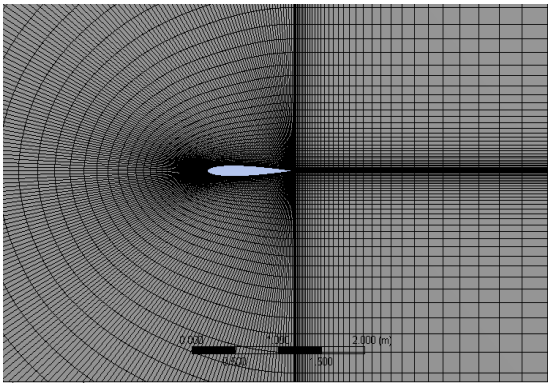

Fig. 7. Close view of the problem mesh

5. Validation

In this section, to validate the independence of the grid and the desired geometry, fixed airfoil simulations are solved and the results of pressure coefficients and shell friction for S-A, RNG and LES models are compared with the experimental results of [14].

In Fig. 8 of the LES model, the pressure coefficient decreases as it approaches the tip of the airfoil nose. In fact, the value of the pressure coefficient is high due to the maximum pressure. Another reason for this is due to the non-slip condition in the airfoil tip area, which indicates that the velocity in the layers attached to the airfoil wall is zero. In fact, according to the Bernoulli equation, velocity and acceleration are inversely related to particles passing through

flow lines. In S-A and LES models, the maximum value between the coordinates [+0.4, +0.6] is predicted. This is more consistent with the experimental results in terms of fluid behavior.

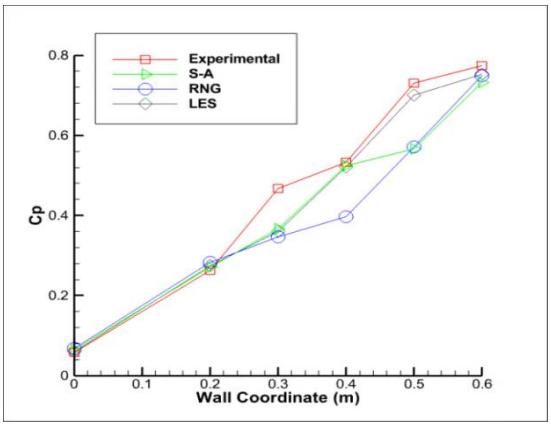

Fig. 8. Figure 8. Comparison of pressure coefficient change diagrams for the results obtained for S-A, RNG, LES and experimental results [14]

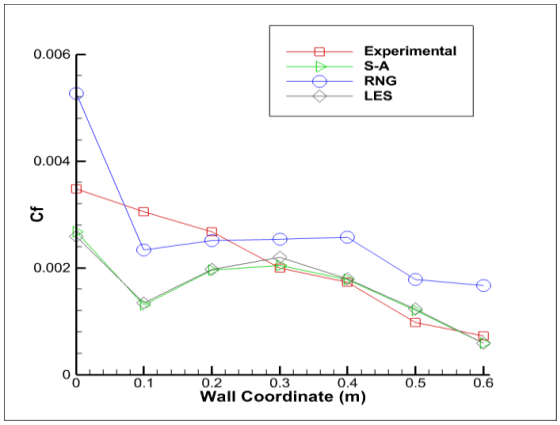

Fig. 9. Comparison of friction coefficient change diagrams for the results obtained for S-A, RNG, LES and experimental results [14]

Fig. 9 shows the maximum friction coefficient for the LES model of the first region, which is near the tip of the airfoil and has a large curvature, and the amount of friction is reduced along the airfoil path. For the RNG model, the value of Cf changes along the path of the wall with a slope, the maximum value of which is predicted to be approximately 0.6 m. In fact, the two models, S-A and LES, it is somewhat similar to the experimental Data.

6. Results

6.1. Fixed Airfoil Results

Fig. 10 and Fig. 11 show the drag and lift coefficient values for the RANS and LES models, respectively. The drag coefficient has been increased in all models. However, the lift coefficient for the RNG and SST models decreases after the 5 ° angle, so the 10 ° angle rises again and has increased for the RSM, S-A, and LES models, so the airfoil for these boundary conditions in the RNG and SST models is different after 5 ° angle.

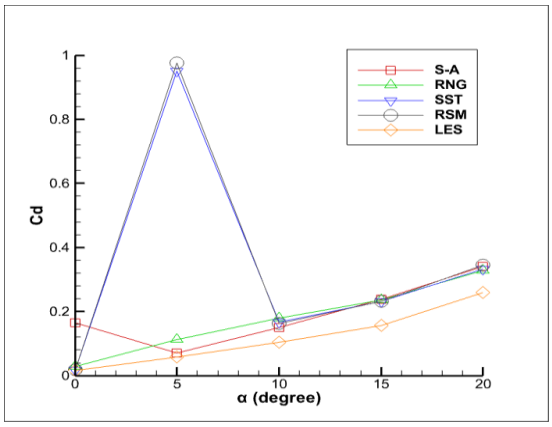

Fig. 10. Comparisons of fixed airfoil drag coefficient change diagrams

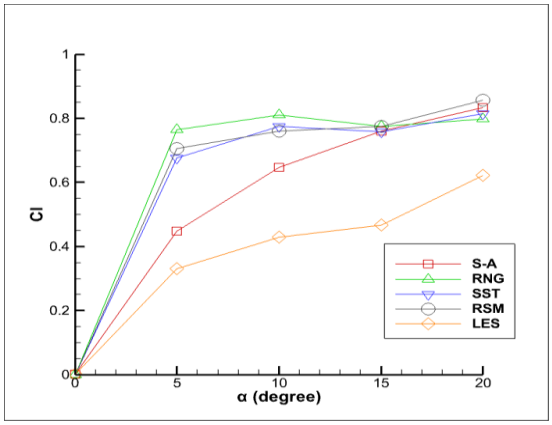

Fig. 11. Comparisons of fixed airfoil lift coefficient diagrams

6.2. Rotating Airfoil Results

In Fig. 12 and Fig. 13, the drag and lift coefficient has increased as the attack angle increases.

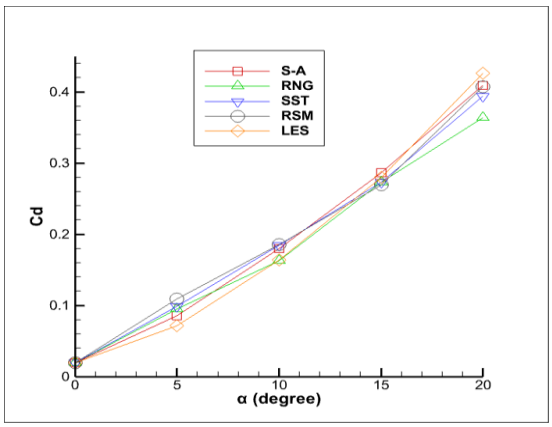

Fig. 12. Comparison of rotating airfoil drag coefficient diagramdiagrams

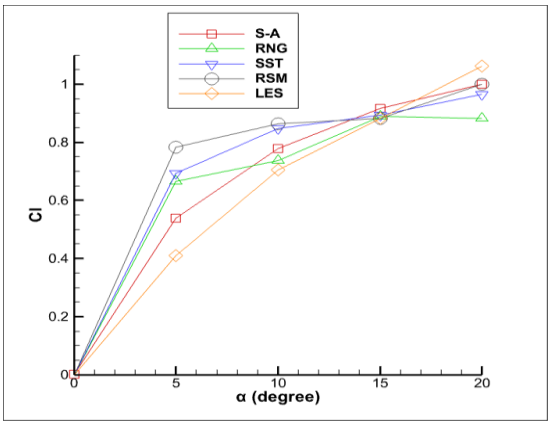

Fig. 13. Comparison of rotation airfoil lift coefficient diagram

The value of the coefficient of friction is directly related to the shear stress. According to Fig. 14, the shear stress on the wall has the highest value at the beginning and the lowest value at the end of the wall coordinates, so the S-A and LES models have a more accurate prediction than the other models [16].

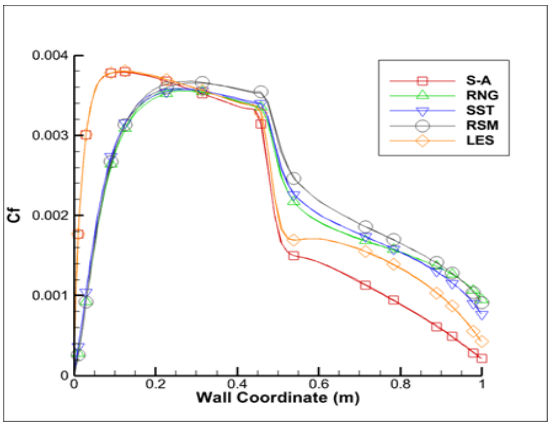

Fig. 14. Comparison of diagrams of changes in friction coefficient of rotating airfoil at 0 ° attack angle

In Fig. 15 the value of the pressure coefficient for all five models of the RANS and LES methods is estimated to be the same. This value is at first the highest, then up to about 0.4 m of descending wall and rising again.

In these diagrams of RANS and LES models, it is observed that the single-equation models S-A and LES have a big difference in predicting the coefficient of friction. In fact, the predictions made by the S-A and LES models make sense in many important and essential variables in aerodynamic problems. The single-equation models S-A and LES are accurate enough in predicting separation point, lift and drag coefficient, pressure coefficient and friction.

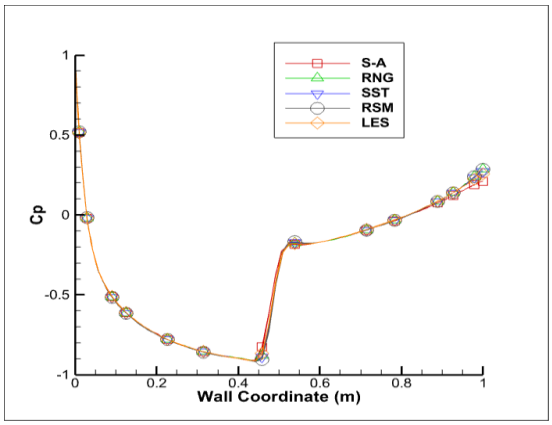

Fig. 15. Comparison of diagram of changes in pressure coefficient of rotating airfoil at 0 ° attack angle

6.3. *Comparison of Flow around Fixed and Rotating Airfoils*

In Fig. 16 and Fig. 17, the drag coefficient of a rotating airfoil is very different from that of a fixed airfoil due to the Coriolis acceleration and centrifugal acceleration terms.

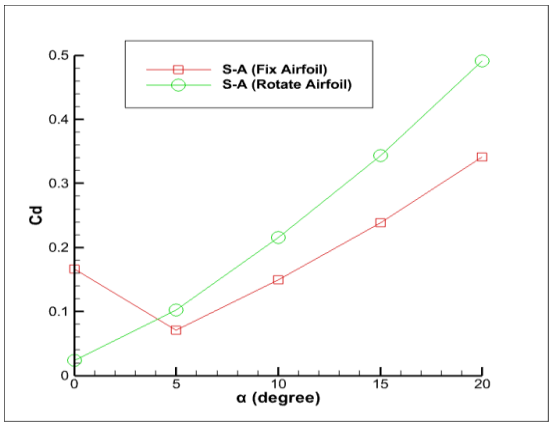

Fig. 16. Comparison of fixed and rotating airfoil drag coefficient diagrams of S-A model

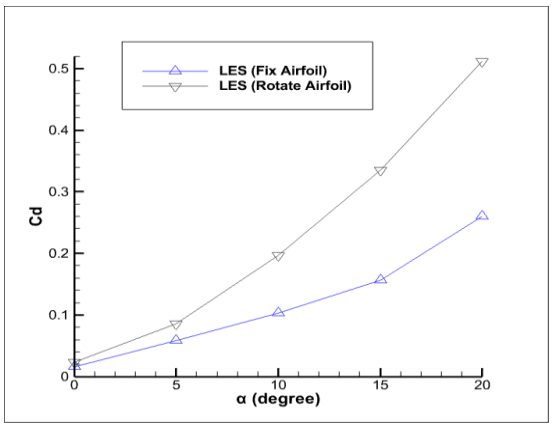

Fig. 17. Comparison of fixed and rotating airfoil drag coefficient diagrams of LES model

Fig. 18 and Fig. 19 show the value of the lift coefficient for different angles in comparison of two modes of fixed airfoil and rotating airfoil with two models S-A, and LES. The rotational airfoil lift coefficient is much more predicted due to the addition of centrifugal acceleration terms and Coriolis acceleration to the spring term of the momentum transfer equation.

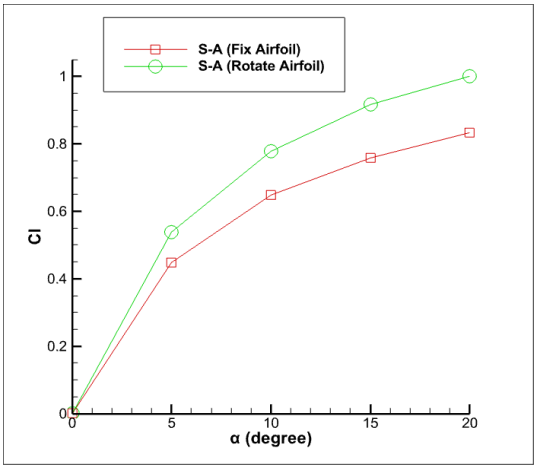

Fig. 18. Comparison of fixed and rotating airfoil lift coefficient diagrams of S-A model

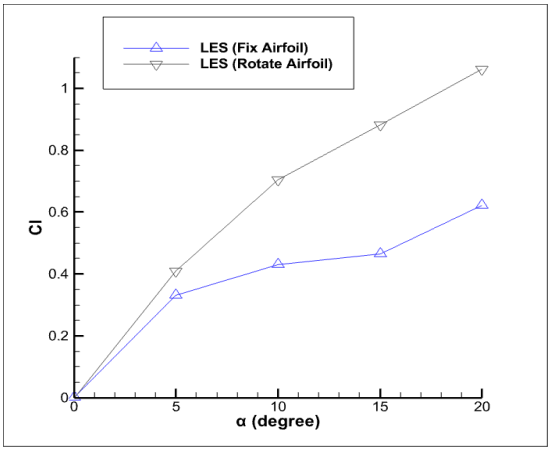

Fig. 19. Comparison of fixed and rotating airfoil lift coefficient diagrams of LES model

In Fig. 20, The temperature contour around the moving airfoil shows that the temperature is the same in different RANS and LES methods, and the method does not cause any change in temperature.

The vortex core is a special example of an isolated surface that shows only vortices. The Fig. 20 clearly shows how different amounts of vertigo, vortices, have grown and disappeared. Also, there is a large angular velocity at the escape edge and the maximum value in the LES method.

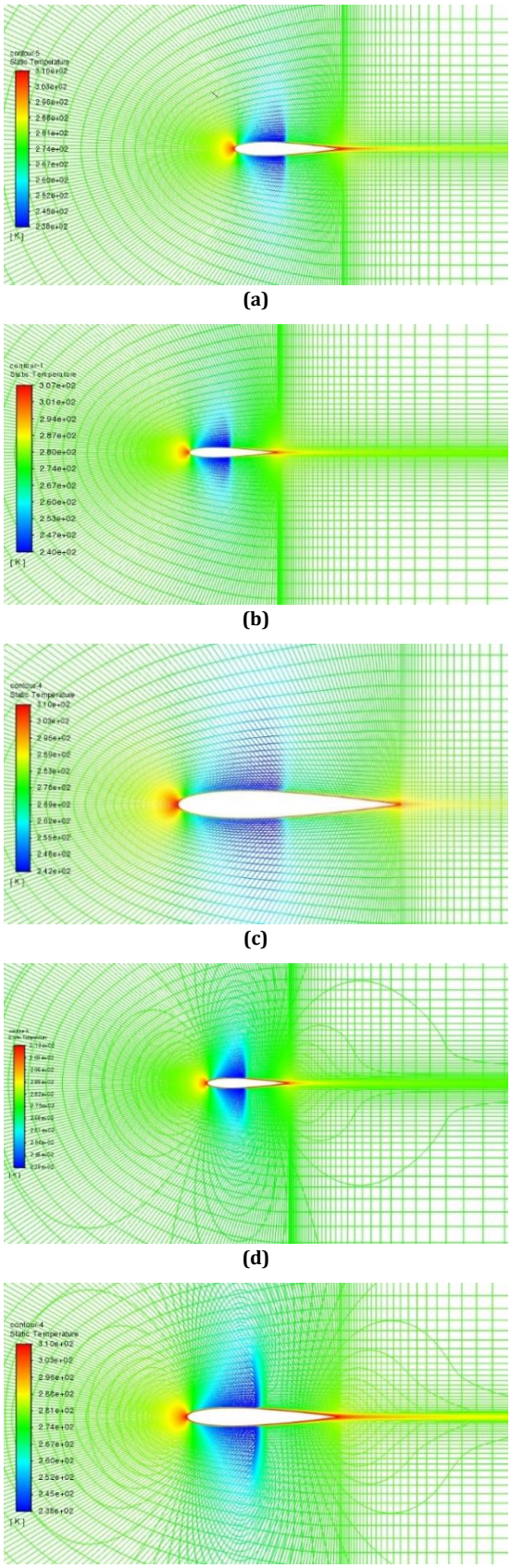

(a) **(b)** **(c)** **(d)** **(e)**

Fig. 20. Temperature contour rotating airfoil Models: a) S-A; b) RSM; c) RNG; d) SST; e) LES

6.4. Impeller Results

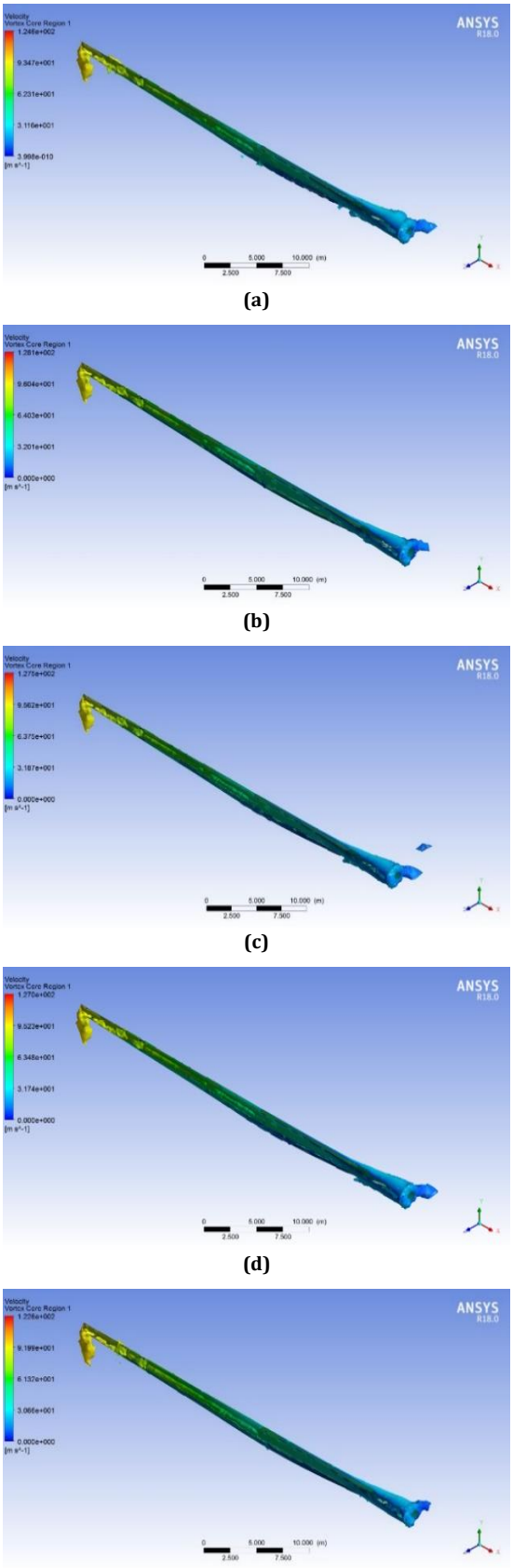

(a)

(b)

(c)

(d)

(e)

Fig. 21. Vortex core for velocity in impeller of fluid rotational power for 4.41812 s-1 Models: a) S-A; b) RSM; c) RNG; d) SST; e) LES

According to the diagram in Fig. 21, the S-A method bears more pressure than the other RSM, SST, RNG and LES methods. In the S-A method, between the points Z = (- 200, 0), the ascending graph and the point Z = 0, the pressure reaches the lowest numerical value, i.e. zero, and then ascends again. The maximum numerical value of pressure is at point Z = 10. In RSM, SST, RNG, and LES methods, numerical values have a limited difference. In these methods, the numerical value of pressure between point Z = (-200, 0) is almost zero, and at point Z = 0, the slope of the graph becomes negative, and then the slope of the graph becomes ascending. The S-A model is a single equation that involves less physics than vortices. In contrast to the two-equation models, large physics vortices contain more than vortices, so the pressure difference between the S-A model and other models is very large.

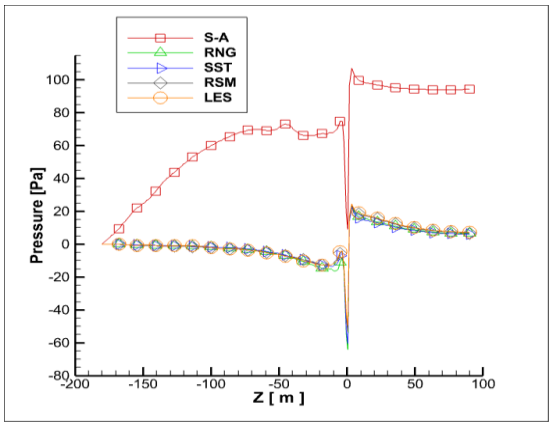

Fig. 22. Comparison of pressure diagram around the impeller for RANS and LES models

According to Table 2, the maximum is the amount of torque in the LES method and the minimum is the amount of torque in the S-A method.

Table 2. Comparison of torque on the impeller

Model	Torque (N.m)
S-A	88381
RNG	116102
SST	93067
RSM	163091
LES	172116

Fig. 23 Velocity contours is extracted with different turbulent models; the value of maximum velocity in LES modeling is greater than other temporal averaging. Therefore, modeling of small scale can concluded better simulation relative the other calculations.

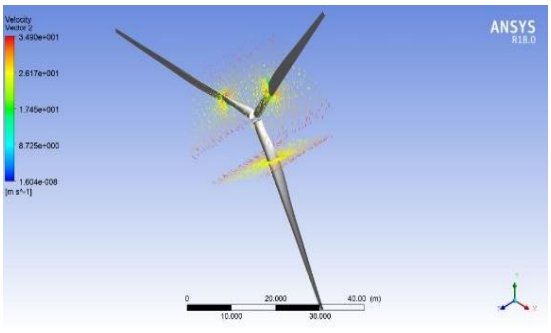

(a)

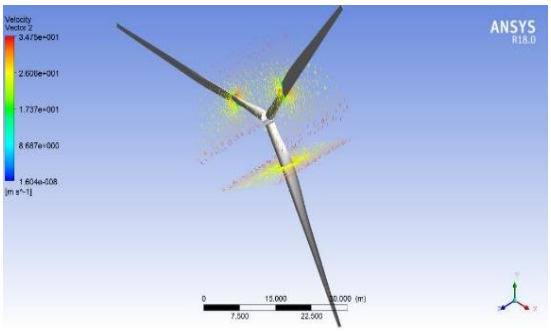

(b)

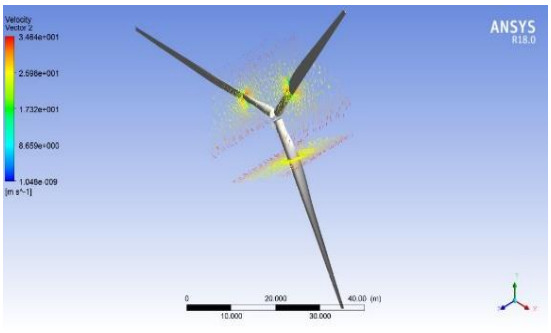

(c)

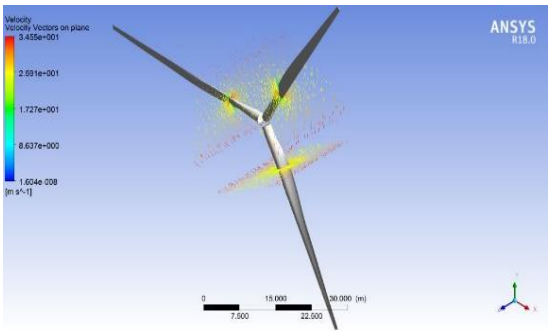

(d)

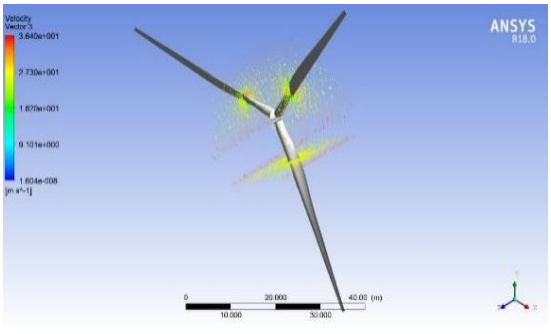

(e)

Fig. 23. Speed Contour Propeller Models: a) S-A; b) RSM; c) RNG; d) SST; e) LES

7. Conclusions

In this paper, the flow around the fixed NACA0012 airfoil and the circular motion and three-dimensional state of the impeller are investigated by RANS and LES methods. It was observed that the results obtained from the LES method for lift and drag coefficients, as well as the torque and mass flow rate resulting from the three-dimensional state of the impeller, are more physical phenomena contents such as large-scale and small scale modelling with subgrid small-scale modeling than the RANS method and this method has physical effects related to vortices, Coriolis acceleration and demonstrates centrifugal flow in airfoils. In this regard, the simulation method LES and RANS in order to simulate the flow around the NACA0012 airfoil, different modes of fixed and rotating airfoil with different angle of attack and 3D impeller mode have been implemented. Lift coefficient, drag coefficient, torque and mass flow of S-A, RNG, SST, RSM and LES models are compared. The net mass rate will be different in the above methods. In RANS methods, the value of the net mass rate is negative, that is, loss of mass rate occurs, but in the LES method, the value of the net mass rate is positive. The highest net mass rate is related to the LES method and in RANS models, the reversed flow is observed. According to the results, the effects of body forces in energy equation or thermal dissipation under circular motion are important in comparison with experimental data. Comparison of fixed and rotating airfoil lift coefficient diagrams with LES model are shown that lift coefficient in fixed airfoil is two times relative to rotating airfoil, also comparison of torque on the impeller with different turbulent models are varying from 88381 to 172116.

Thermal dissipation and work of body force in energy equation (work of Coriolis and centrifugal body force) causes the stability in numerical scheme.

Nomenclature

C_d	Drag coefficient
C_f	Friction coefficient
C_l	Lift coefficient
C_p	Pressure coefficient
F	Source sentence
F_l	Flux vector
F_v	Flux vector

k	Energy kinetic turbulence, m^2/s^2
p	Pressure, Pa
$\overline{P}$	Medium pressure, Pa
R	Radius, m
T	Temperature, K
T	Time, s
u	x-Velocity, m/s
v	y-Velocity, m/s
α	Attack angle, Deg
∇	Gradient
ε	Rate loss turbulence, m^2/s^3
μ	Fluid viscosity, Pa.s
μ_{eff}	Effective viscosity
ρ	Fluid density, kg/m^3
r_{eff}	Effective penetration coefficient
Q	Source term vector
U,V,W	Large scale (filtered quantities)
φ	Subgrid small scale quantities
ω	Angular velocity, rad/s

Funding Statement

This research did not receive any specific grant from funding agencies in the public, commercial, or not-for-profit sectors.

Conflicts of Interest

The author declares that there is no conflict of interest regarding the publication of this article.

References

[1] Silva, L. J., & Wolf, W., 2023. Analysis of adverse pressure gradient effects in the boundary layer of a NACA0012 airfoil at high angles of attack. In *AIAA Aviation 2023 Forum,* p. 4007.

[2] Silva, L. J., & Wolf, W. R., 2024. Embedded shear layers in turbulent boundary layers of a NACA0012 airfoil at high angles of attack. *International Journal of Heat and Fluid Flow*, 109353.

[3] Steenwijk, B., & Druetta, P., 2023. Numerical Study of Turbulent Flows over a NACA 0012 Airfoil: Insights into Its Performance and the Addition of a Slotted Flap. *Applied Sciences*, *13*(13), 7890.

[4] Sharma, D., & Goyal, R., 2022. Numerical Simulation and Validation of NACA0012 Airfoil to Predict Its Performance During the Stalling Condition. In *Conference on Fluid Mechanics and Fluid Power,* pp. 173-184, Singapore: Springer Nature Singapore.

[5] Rahimi, M., Parsajou, B., & Vajdi, M., 2022. Numerical Investigation of Convective Heat Transfer from a Horizontal Plate Due to the Oscillation of a Vertically Oriented Blade. *Journal of Heat and Mass Transfer Research*, *9*(2), 111-120.

[6] Mitchell, S., Ogbonna, I., & Volkov, K., 2021. Aerodynamic characteristics of a single airfoil for vertical axis wind turbine blades and performance prediction of wind turbines. *Fluids*, *6*(7), 257.

[7] Balakumar, P., 2020. Wall-Modeled LES for flows over an NACA-0012 Airfoil. In *AIAA Scitech 2020 Forum* ,p. 1810.

[8] Zhao, M., Wan, D., & Chen, G., 2019. Comparison of SST k-ω and Smagorinsky Model in Cavitation Simulation around NACA0012. In *ISOPE International Ocean and Polar Engineering Conference* , ISOPE.

[9] Oukassou, K., El Mouhsine, S., El Hajjaji, A., & Kharbouch, B., 2019. Comparison of the power, lift and drag coefficients of wind turbine blade from aerodynamics characteristics of Naca0012 and Naca2412. *Procedia Manufacturing*, *32*, pp. 983-990.

[10] Cariglino, F., Ceresola, N., & Arina, R., 2014. External aerodynamics simulations in a rotating frame of reference. *International Journal of Aerospace Engineering*, *2014*(1), 654037.

[11] Eleni, D. C., Athanasios, T. I., & Dionissios, M. P., 2012. Evaluation of the turbulence models for the simulation of the flow over a National Advisory Committee for Aeronautics (NACA) 0012 airfoil. *Journal of Mechanical Engineering Research*, *4*(3), 100-111.

[12] Sipilä, T., 2012. RANS analyses of cavitating propeller flows: Licentiate thesis.

[13] Qiu, W., Peng, H., Liu, L., Mintu, S., & Hsiao, C. T., 2010. Effect of turbulence modeling on RANS computation of propeller tip vortex flow. In *ISOPE International Ocean and Polar Engineering Conference* (pp. ISOPE-I). ISOPE.

[14] Abbott, I. H., & Von Doenhoff, A. E., 2012. *Theory of wing sections: including a summary of airfoil data*. Courier Corporation.

[15] Asadi, B. Asadi, M., 2012. A numerical simulation of a compressible fluid flow around an airfoil in a circular motion, *in Mechanical Engineering*, Iran , Shiraz University, pp. 6-14.

[16] Schobeiri, M. T., 2010. *Fluid mechanics for engineers: a graduate textbook*. Springer Science & Business Media.

[17] Shojaeifar, M.H., 2012 Introduction to turbulent flows and its modeling, *University of Science and Industry*.

[18] Piomelli, U., 1994. Large-eddy simulation of turbulent flows, Department of Theoretical and Applied Mechanics. College of Engineering.

[19] Anderson, J., 2011. *EBOOK: Fundamentals of Aerodynamics (SI units).* McGraw hill.

[20] Ochoa, J. S. and Fueyo, N., 2004, May. Large Eddy Simulation of the flow past a square cylinder. In *International PHOENICS Conference, Melbourne, Australia*.